OBSERVATION OF GRAVITY WAVES IN A BOREAL FOREST

X. LEE[1], H. H. NEUMANN[2], G. DEN HARTOG[2], J. D. FUENTES[3], T. A. BLACK[4], R. E. MICKLE[2], P. C. YANG[4] and P. D. BLANKEN[4]
[1]*School of Forestry and Environmental Studies, Yale University, New Haven, Connecticut, CT 06511 U.S.A.*
[2]*Atmospheric Environment Service, Environment Canada, Toronto, Ontario, Canada*
[3] *Department of Environmental Science, University of Virginia, Charlotteville, Virginia, U.S.A.*
[4]*Department of Soil Science, University of British Columbia, Vancouver, British Columbia, Canada*

(Received in final form 23 December, 1996)

Abstract. In this paper we report the results of the analysis of two 60-min wave events that occurred in a boreal aspen forest during the 1994 BOREAS (Boreal Ecosystems-Atmosphere Study) field experiment. High frequency wind and temperature data were provided by three 3-D sonic anemometer/thermometers and fourteen fine-wire thermocouples positioned within and above the forest. Wave phase speeds, estimated from information revealed by spectral analysis and linear plane wave equations, are 2.2 and 1.3 m s^{-1} for the two events. The wavelengths are 130 m and 65 m respectively and are much larger than the vertical wave displacements. There is strong evidence from the present analysis and from the literature supporting our postulate that these waves are generated by shear instability. We propose that wind shear near the top of the stand is often large enough to reduce the gradient Richardson number below the critical value of 0.25 and thus is able to trigger the instability. When external conditions are favorable, the instability will grow into waves.

Key words: Canopy waves, BOREAS, Shear instability, Phase speed, Forest

1. Introduction

This study is motivated by the need to understand atmosphere-forest exchange of trace gases at night when plant physiological and soil processes can give rise to fluxes with magnitudes comparable to daytime values. Current ability to quantify these fluxes is however hindered by a lack of good knowledge of nocturnal atmospheric processes, and in particular, those related to wavelike motions. In our previous experiments we found that wave motions are the normal state of affairs over forest canopies: Wave episodes of various intensities were observed over 30% of the nights at our temperate (Lee et al., 1996) and boreal (Black et al., 1996) forest sites. For convenience of discussion, we shall loosely refer to waves that occur within and immediately above a vegetative canopy as canopy waves. The labeling here is semantic only and does not reflect the dynamics of wave motion.

Analysis of a number of wave episodes reveals that canopy waves possess a dominant wave period on the order of 1 min, which is much shorter than that of waves generated in the upper boundary layer. This distinction suggests that canopy waves are generated locally rather than being waves that have propagated downward from higher altitudes.

In a previous paper we discussed some implications of wave motions in transporting CO_2 over a temperate forest (Lee et al., 1996). In this paper we extend the

Boundary-Layer Meteorology **84:** 383–398, 1997.

analysis using a new data set, (1) to provide a better description of wave features including estimates of key wave parameters such as phase speed and wavelength, and (2) to offer a plausible explanation for mechanisms of the wave generation. The data set was obtained in 1994 as part of the BOREAS (Boreal Ecosystem-Atmosphere Study) field campaign. The data set is unique in that a set of 14 fine wire thermocouples was deployed at small vertical increments in addition to three 3-d sonic anemometer/thermometers so that detailed structure of air motion can be inferred. In this paper a case study approach is adopted as our data analysis strategy because it is a necessary first step towards a better understanding of wave climatology and wave dynamics. Two 60-min wave events (events A and B), having different appearances, are selected out of a large number of wave episodes for a detailed examination. Event A (2:22–3:22 local time, July 13) is chosen because periodic motions are evident at all observation levels. On the other hand, during event B (2:39–3:39 local time, August 4) clearly defined wave motions are confined to a thin layer near the treetops. In addition, event B is the only one that partially overlaps with a tethersonde profile observation (see below).

2. Experimental Methods

2.1. SITE

The site (53.7° N, 106.2° W) is located in the southern part of Prince Albert National Park, Saskatchewan, Canada. The forest is an extensive stand of aspen trees about 21 m tall. The overstory leaf area index was 1.5 during the growing season (June–August). Most of the overstory leaves were found above z = 15 m. The forest floor was covered by thick understory vegetation about 2 m tall and with a leaf area index of 3.2 during the growing season.

2.2. INSTRUMENTATION

The key instrumentation was an eddy correlation (EC) system, which included three sonic anemometer/thermometers (Kaijo Denki Co., Ltd., Japan, models TR310 and TR61AB), mounted permanently at z = 5.5, 27.7 and 39.1 m on a double-scaffolding tower, and several fast-response gas analyzers. A desk-top computer was interfaced with an A/D system (National Instruments Co., Austin, TX, model AT-MIO-16X, multiplexed to 32 differential channels) to sample all signals at 100 Hz and then average down to 20 Hz for on-line data processing. Digital averaging was intended to minimize possible high frequency electrical noise. All 20 Hz data were saved on digital tapes for post-field data analyses. The EC system was in operation continuously from February to September 1994.

A fine-wire thermocouple (TC) profile system was mounted on the same tower. Sensors (chromel-constantan, 26 μm diameter) were positioned at z = 0.1, 1.0, 2.2, 4.1, 6.4, 9.5, 12.6, 15.7, 18.8, 21.9, 25.0, 27.7, 31.4 and 39.1 m. Their signals

were recorded at 5 Hz by a data logger (Campbell Scientific, Inc., Logan, UT, model CR7). Mean temperature profiles were calculated after the experiment from the high frequency data. The separation between the top TC sensor and the top sonic unit was less than 10 cm, thus allowing us to synchronize EC and TC data by matching the two temperature traces later. The TC system was in operation for most of the period between June and September 1994. Because its sensors were closely spaced, data from this system provide detailed information about the vertical structure of wave motions.

A tethersonde (Atmospheric Instrumentation Research, Inc., Boulder, CO, model TS-3A-SP) carrying a set of wind, temperature, humidity and ozone sensors was used to probe the air layer with increments of 3 m up to z = 300 m. The operating site was a small clearing about 100 m away from the main tower. This system was operated mostly in the daytime, with a few runs made at night, one of which partially overlapped with event B.

Details of supporting measurements can be found in Black et al. (1996).

3. Theory

3.1. WAVE AMPLITUDE AND FREQUENCY

Information revealed by Fourier analysis is used to define physical properties of wave motions. To be consistent with the sampling frequency of the TC system, a 4-point block averaging is applied to the time series of the EC system. Discrete Fourier transformation is applied to the full 60-min time series and spectra and cospectra are formed for each wave event. Prior to the transformation signals are detrended and then tapered with a Hanning window. The power spectrum (S_x) and cospectrum (C_{xy}) are defined such that

$$\sigma_x^2 = \int_0^\infty S_x \, \mathrm{d}f,$$

and

$$\overline{x'y'} = \int_0^\infty C_{xy} \, \mathrm{d}f,$$

where σ_x is the standard deviation of x, $\overline{x'y'}$ the covariance between x and y and f is the natural frequency in Hz. The phase spectrum is determined from

$$\phi_{xy} = \tan^{-1}(Q_{xy}/C_{xy}),$$

where Q_{xy} is the quadrature spectrum.

For both wave events, the peak frequency of the power spectrum of the vertical velocity at z = 27.7 m is used as the wave frequency (f_w). Because the record used

in the Fourier analysis is relatively long compared to the wave period, the resulting resolution of the wave period estimate ($1/f_w$) is better than 1 s. For event A, peak frequencies for all other EC and TC time series agree with the f_w value to within 0.001 Hz, while for event B, peak frequencies for time series recorded in the lower half of the stand show some scatter as a result of weak periodic motion there.

Two methods have been used previously to quantify wave amplitudes. De Baass and Driedonks (1985) and Busack and Brümmer (1988) used standard derivations from the Reynolds averaging as amplitude estimates. The obvious drawback of this method is that it does not isolate wave motion from either low-frequency trends or background turbulence. A second method estimates the amplitudes from the waveforms determined by a phase-averaging procedure (Finnigan et al., 1984). Because of the non-sinusoidal nature of our time series, this method has been found to be very sensitive to the starting time of the phase averaging.

In the present study we use the peak value of $(fS_x)^{0.5}$ as an approximation to the wave amplitude of x. This method is most accurate when a wave frequency can be identified unequivocally and sample size of the spectrum in the low frequency range is large, as is the case here. Obviously the tapering will reduce the spectral peak by a certain amount. This however should not be a major concern because good agreement between the integrated spectrum energy and the corresponding Reynolds variance exists for most time series.

3.2. PHASE SPEED

Two methods are used to infer wave phase speed. The first method relies on the linear wave equation for potential temperature (θ) in an air layer free of plant elements, as

$$\frac{\partial \tilde{\theta}}{\partial t} + \overline{u}\frac{\partial \tilde{\theta}}{\partial x} + (\frac{\overline{\theta}}{g}N^2)\tilde{w} = 0, \tag{1}$$

where u is the x component of the horizontal velocity, w the vertical velocity component, g the gravitational acceleration, N the Brunt-Väisälä frequency, and overbar and tilde denote mean and wave components of a quantity respectively. The coordinate system is defined such that z is vertical and x is aligned with the azimuthal direction of wave propagation. This direction is found from wave-associated wind speed and direction fluctuations (Gossard and Munk, 1954) to fall within 18 degrees of the mean wind direction. Thus in the following we will orient the x-coordinate along the mean wind direction (longitudinal direction).

Expressing wave amplitudes in the form of a plane wave

$$\tilde{a} = \hat{a}(z)\exp[\mathrm{i}(kx - \sigma t)], \tag{2}$$

we can transform Equation (1) to

$$A_\theta = \frac{A_w}{[(\overline{u}k - \sigma_r)^2 + \sigma_i^2]^{1/2}}\left(\frac{\overline{\theta}}{g}N^2\right). \tag{3}$$

Here $A_a = \mid \hat{a} \mid$ is the wave amplitude of quantity a, k the wavenumber, and σ (= $\sigma_r + \mathrm{i}\sigma_i$) the complex wave angular frequency. Since the growth rate σ_i is usually small, Equation (3) can be re-arranged to give

$$k \simeq \left(\sigma_r \pm \frac{A_w}{A_\theta} \frac{\overline{\theta}}{g} N^2 \right) / \overline{u}. \tag{4}$$

The negative (positive) sign is chosen if the observation height lies below (above) the critical level, a level at which phase speed c_r is equal to the mean wind speed $\overline{u}$. Estimates of A_θ, A_w and $\sigma_r (= 2\pi f_w)$ provided by the above spectral analysis are used to find k from Equation (4). Phase speed is then given by

$$c_r = 2\pi f_w / k. \tag{5}$$

The second method is taken from Hooke et al. (1973), who suggested the following relation

$$\frac{N^2}{(k\overline{u} - \sigma_r)^2} - 1 = \left(\frac{A_u}{A_w} \right)^2. \tag{6}$$

This equation can be re-arranged to give wavenumber and therefore phase speed.

4. Results and Discussion

4.1. EVENT A

Table I lists Reynolds statistics for the two wave events. These statistics include both wave and turbulence contributions. Except for sensible heat near the forest floor, all fluxes are negative (directed downward).

Visual inspection of the data of event A indicates that periodic patterns are clear and last the whole duration. A segment of the TC time series at selected heights is plotted in Figure 1 (left panel). Note that these are 1-s averaged data and hence high frequency turbulence has been smoothed out. The periodic pattern is evident at all levels. Two peaks exist in the amplitude profile of the temperature wave (Figure 2), the dominant one above the canopy which is a critical-level phenomenon as explained below, and the secondary peak in the trunk space probably because air can move freely there.

Ramp-like structures are evident in the air layer near the treetops, perhaps as a result of non-linear interactions of the wave and turbulence (Einaudi and Finnigan, 1993) or a non-constant mean temperature gradient (Maitani, 1989). The synchronous occurrence of ramps near the canopy top and wavelike motions above was also reported by Paw U et al. (1992) and Lee et al. (1996). Data presented here suggest that there is indeed no clear distinction between the two forms of motions:

Table I
Reynolds statistics from the EC system for the two wave events

Event	z m	$\overline{u}$ m s^{-1}	σ_u m s^{-1}	σ_w m s^{-1}	σ_T °C	$\overline{u'w'}$ m^{2}s^{-2}	$\overline{w'T'}$ °C m s^{-1}
A	39.1	2.93	0.74	0.37	1.00	−0.060	−0.021
	27.7	1.53	0.62	0.39	0.68	−0.103	−0.031
	5.5	0.48	0.19	0.08	0.28	−0.001	0.002
B	39.1	2.92	0.32	0.14	0.36	−0.009	−0.010
	27.7	1.56	0.47	0.20	0.48	−0.031	−0.030
	5.5	0.18	0.12	0.05	0.27	−0.003	0.003

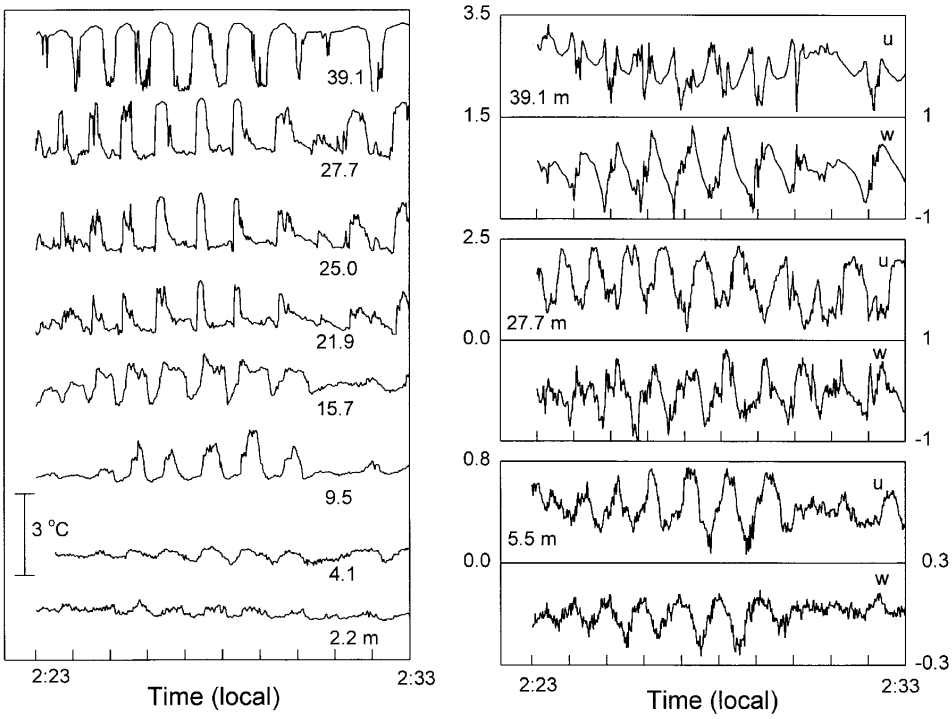

Figure 1. Ten-minute time series of temperature (°C), longitudinal (u, m s^{-1}) and vertical velocity (w, m s^{-1}) from event A.

phenomena labeled by some people as inverse ramps may also be regarded by others as components of wave oscillations.

The u and w time series (Figure 1, right panel) show a similar wave amplitude. In comparison to the lower two levels, the traces at z = 39.1 m appear smoother. Another interesting feature is that the u time series at z = 39.1 m is comprised of motions of several distinct periods. Spectral analysis reveals three peaks at 0.0081,

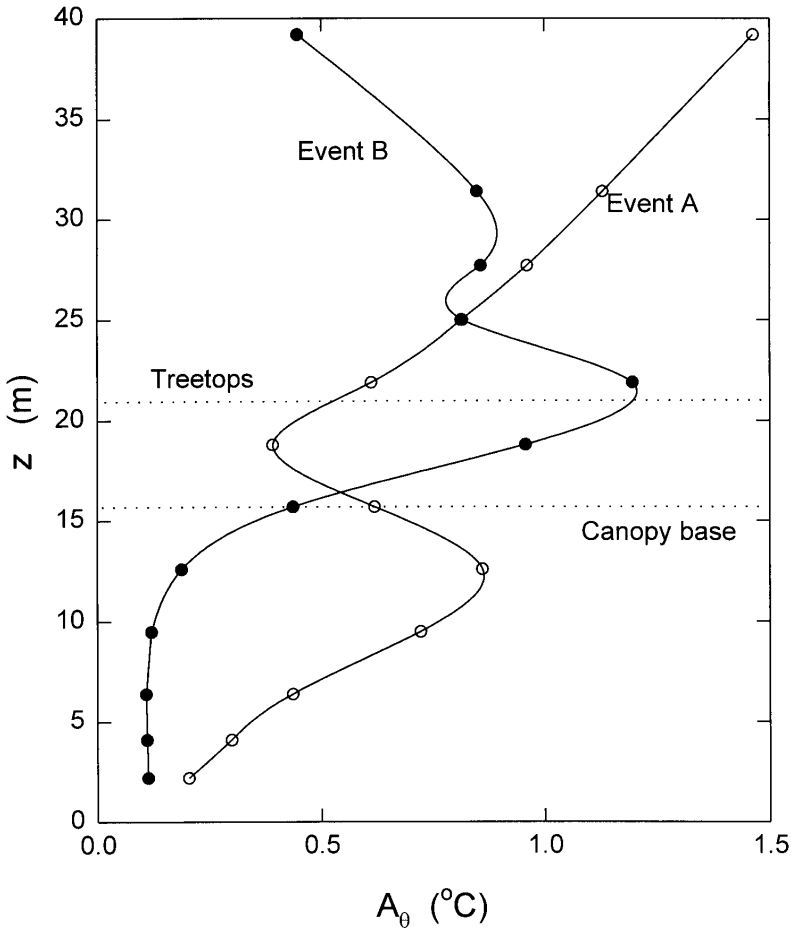

Figure 2. Profiles of wave amplitude of temperature for event A and event B.

0.0125 and 0.0158 Hz, with corresponding fS_u values of 0.47, 0.45 and 0.69 $m^2\ s^{-2}$ respectively.

Finnigan (1988) noted that it is very difficult to separate waves in the upper boundary layer from turbulence using frequency spectra. The difficulty arises from the fact that these waves are rarely monochromatic (e.g., de Baas and Driedonks, 1985) and from the lack of a spectral gap in the frequency domain separating the two forms of motions. In contrast, canopy waves can be detected quite easily by spectral analysis. For example, power spectra at z = 27.7 m (Figure 3) clearly indicate a wave frequency (f_w) of 0.0169 Hz or a wave period of 59 s which is close to values reported elsewhere (Fitzjarrald and Moore, 1990; Lee et al., 1996). Spectra at all other levels also peak at roughly the same frequency. The success of the spectral method here is accounted for in two ways: First, unlike waves in the upper boundary layer, canopy waves often possess a single dominant wave period;

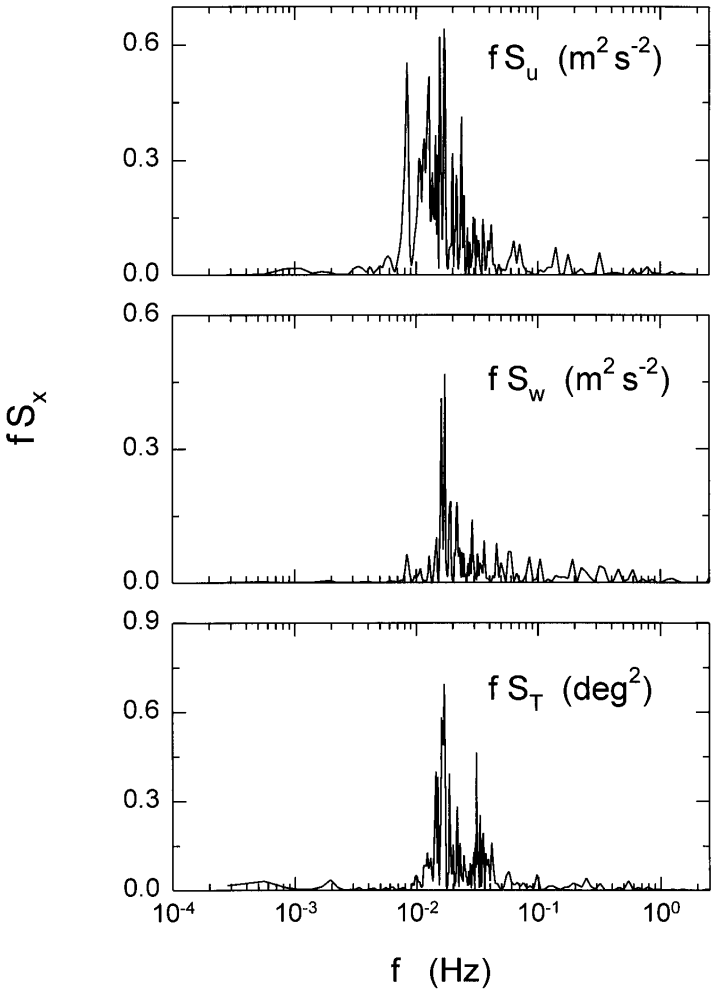

Figure 3. Power spectra of longitudinal and vertical velocities and temperature at z = 27.7 m for event A.

Second, there exists a separation between the wave frequency and the frequency of the most energetic turbulent eddies in a forest. The separation is particularly large for the vertical velocity. Lee (1996) showed that the frequency of the w spectrum peak due solely to turbulence depends on air stability, canopy height (h) and wind speed at the treetops (u_h). In moderately stable air with typical values of 20 m for h and 1 m s^{-1} for u_h, this peak frequency is about $3u_h/h$ or 0.15 Hz, which is one decade larger than the expected wave frequency.

Key wave parameters are summarized in Table II. The wave frequency is lower than $N/2\pi$, in agreement with data presented by Lee et al. (1996) and Fitzjarrald and Moore (1990). Estimates of the phase speed (c_r) by the two methods (Equations

Table II
Wave parameters

Event	f_w	z	N	A_u	A_w	A_θ	c_r Eq. (5)	c_r Eq. (6)
	Hz	m	Hz	m s^{-1}	m s^{-1}	°C	m s^{-1}	m s^{-1}
A	0.0169	39.1	0.0590	0.83	0.64	1.49	2.07	2.21
		27.7	0.0428	0.80	0.68	0.83	2.61	2.07
		5.5	0.0695	0.43	0.15	0.37	1.00	0.52
B	0.0200	39.1	0.0482	0.27	0.24	0.42	2.23	2.32
		27.7	0.0617	0.91	0.30	0.77	1.16	1.45
		5.5	0.0780	0.09	0.08	0.10	0.08	0.12

4 and 6) at the two heights above the canopy agree reasonably well, giving a mean value of 2.2 m s^{-1}. The fact that the c_r value falls in between $\overline{u}$ at z = 39.1 m and that at z = 27.7 m (Table I) suggests the existence of a critical level – the level at which the mean longitudinal wind speed is equal to the phase speed – somewhere between the two observation levels. At the critical level, the amplitude of air density (and therefore air temperature) variations should have a maximum (Einaudi and Finnigan, 1981). The amplitude profile (Figure 2) does not show this maximum, but it is possible that the maximum did occur between z = 31.4 and 39.1 m and the TC system did not have sufficient vertical resolution to detect it.

Errors caused by the exclusion of the growth rate (σ_i) from Equation (4) will depend on the magnitude of σ_i relative to $k(\overline{u} - c_r)$ (see Equation (3)), or in other words, on the vertical separation of the position of observation from the critical level. The consistency in the c_r estimates seems to suggest that the growth rate of event A is very small. This deduction is also supported by the fact that clear periodic patterns last more than 140 cycles without serious breaking, which would be expected had the growth rate been large.

The estimate of c_r at z = 5.5 m must however be discounted because Equation (1) is not valid inside a forest. Within the forest the complete linearized equation for temperature waves should include a term explicitly accounting for the heat exchange between the plant elements and the moving air. The same can be stated about Equation (6) whose complete version should include a term for canopy drag on the waves.

Using a value of 2.2 m s^{-1} for c_r, we arrive at an estimate of 130 m for the wavelength of event A. The wave vertical displacement near the treetops is estimated from $A_\theta/(\mathrm{d}\overline{\theta}/\mathrm{d}z)$ to be about 14 m, thus giving an aspect ratio of 9.3. This ratio is larger than that of most waves in the upper boundary layer and waves in the upper atmosphere (Gossard and Hooke, 1975). This wave is mostly propagating or internal at z = 27.7 and 39.1 m because $\mid \overline{u} - c_r \mid$ is smaller than N/k there (King et al., 1987; Chimonas and Hines, 1986), and must have been trapped or

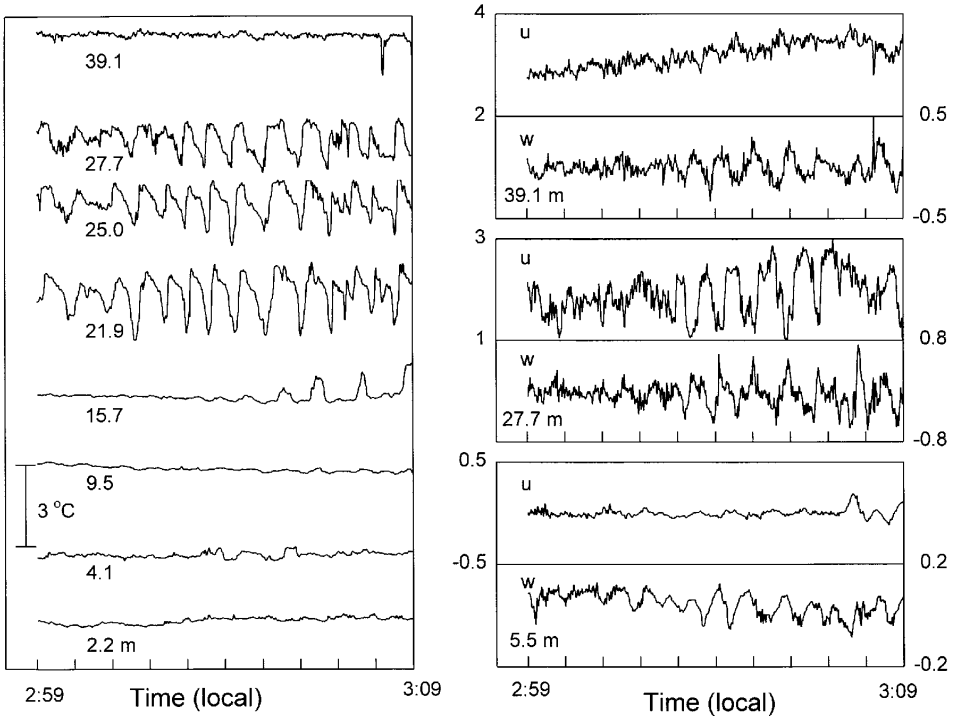

Figure 4. Same as Figure 1 but for event B.

evanescent at higher altitudes (perhaps $z > 2.5h$) where $\mid \overline{u} - c_r \mid$ becomes greater than N/k.

4.2. EVENT B

4.2.1. *General Features*

Turning attention now to event B, we notice one major difference from event A, that is, wavelike motions are clear only in a thin air layer near the top of the stand (Figure 4), with the overall wave magnitude smaller than that of event A (Figure 2). The pattern in Figure 4 resembles the observation of a wave event in an almond orchard (Paw U et al., 1989). The critical level is located this time near the treetops. The vertical velocity power spectrum at z = 27.7 m indicates a wave frequency of 0.0200 Hz or a wave period of 50 s (Figure 5).

There is a large difference between the estimates of the phase speed at z = 27.7 m and 39.1 m. At z = 39.1 m wave motions are rather weak (Figure 4). This, plus the fact that the wave frequency is higher than that of event A, would mean that the signals are 'contaminated' somewhat by turbulence, the contamination being more serious for A_θ and A_u than for A_w. Without the contamination, the ratio A_w/A_θ would have been higher. In other words the contamination has caused an

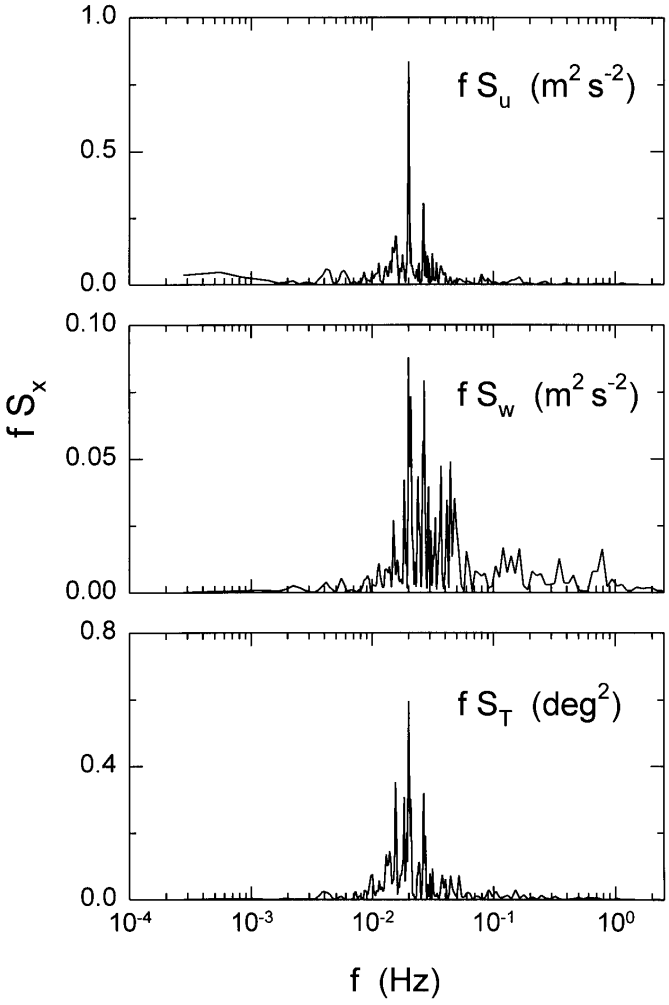

Figure 5. Same as Figure 3 but for event B.

underestimate of k and an overestimate of c_r according to Equations (4) and (5). (The positive sign in Equation (4) is chosen because the critical level lies below the observational point.) For the same reason, Hooke's method would also overestimate c_r. On the other hand, the estimate at z = 27.7 m is less prone to the contamination because wave motions are much stronger there. Additionally, a phase speed of about 1.3 ms^{-1} would most likely match the mean wind speed near the top of the stand, thus producing a wave amplitude maximum as shown in Figure 2.

Using a value of 1.3 m s^{-1} for c_r, the wavelength is estimated to be 65 m. The vertical wave displacement is about 6.2 m, giving an aspect ratio of 10.5. The wave is propagating at z = 27.7 m and evanescent at z = 39.1 m.

4.2.2. *Shear Instability*

Shear instability is a frequent cause of gravity waves in the atmosphere. For this to occur one necessary condition is that the horizontal phase speed must be equal to the background mean wind speed at some height where the gradient Richardson number $Ri = N^2/(\mathrm{d}\overline{u}/\mathrm{d}z)^2$ must be less than 0.25 (Miles, 1961; Howard, 1961). An inflection point is known to exist in the mean wind speed profile near the canopy top. The inflection-point instability is invoked to explain large eddy structures under neutral conditions (Raupach et al., 1989). We postulate that the wind shear is also responsible for the generation of canopy waves. At the inflection point the wind shear reaches a maximum and therefore would be ideal for generating shear instability. Provided that other conditions are favorable, the instability will grow into waves. To support this postulate we have plotted profiles of the background wind and potential temperature from a tethersonde ascent made between 3:37 and 3:57 local time, a period partially overlapped with event B (Figure 6). For the purpose of calculating Ri, the vector wind is first projected to an assumed direction of wave propagation of 105 deg, the mean wind direction within the tower height. The projection is needed for a two dimensional propagaton problem (de Baas and Driedonks, 1985). Polynomials are then fit to the profiles of the wind component and potential temperature. Figure 6c indicates that the minimum Ri is indeed smaller than 0.25 and it occurs near the treetops where the critical level is. Wind shear at all other heights is not strong enough to trigger instability.

No tethersonde profiles are available for event A. Our estimate of Ri based on the tower measurements for the air layer between z = 27.7 and 39.1 m is 0.20, which is also lower than the critical value. The two events analyzed by Lee et al. (1996) for an experiment at the Camp Borden forest also appear to be of shear origin as values of Ri over the treetops are smaller than the critical value.

The shear instability mechanism is based on linear analysis which ignores the effect of waves on background winds. Fitzjarrald and Moore (1990) proposed a competing hypothesis that wavelike motions in their forest were a result of a resonant interaction between a vertically fluctuating pressure gradient force and a deepening stable layer near the canopy top. They also pointed out that wave episodes were always associated with periods of increased wind speed, and presumably decreased Ri, at the canopy top. It is possible that wave motions in their forest were initially triggered by the shear instability. Once formed, they might interact with and modify the background wind and temperature through this resonance mechanism.

The case studied by Maitani (1989) appears to be an exception to our postulate. Maitani observed wave-like fluctuations of temperature and wind velocity within and above a sorghum canopy with a period of 15-20 min. This period is much longer than those found in the literature cited above. We suggest that the low frequency oscillations were a mesoscale phenomenon which was enhanced somehow by plant-air interactions.

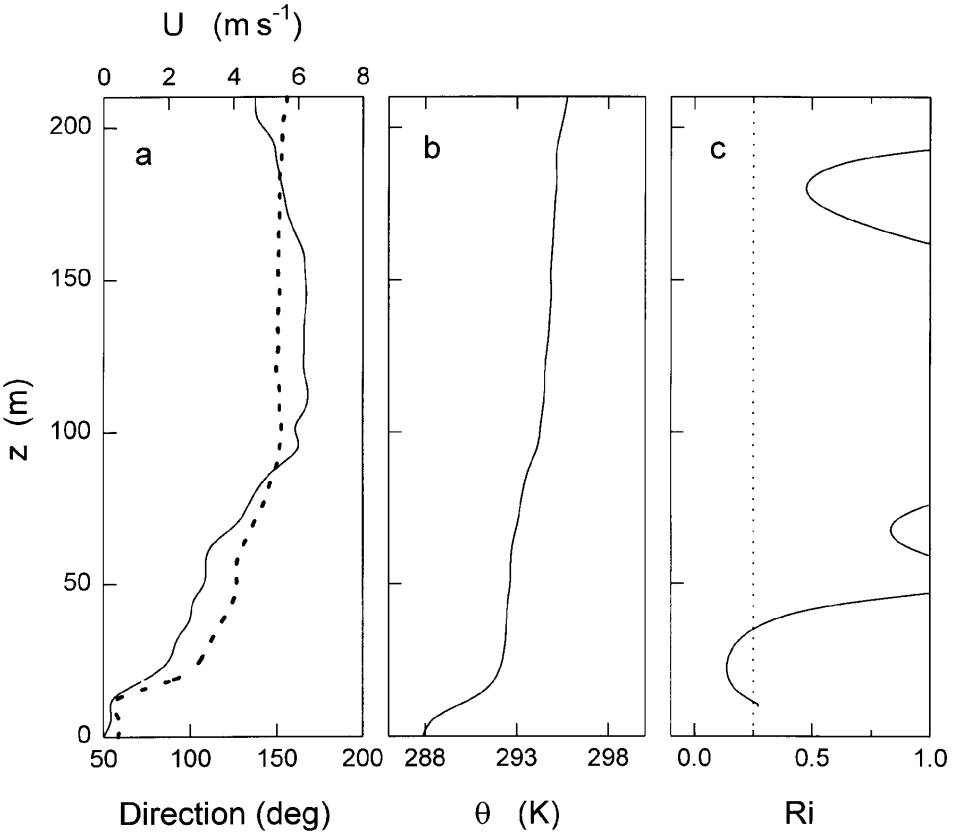

Figure 6. Tethersonde profiles of (a) vector wind speed (solid line) and wind direction (dotted line), (b) potential temperature, and (c) the gradient Richardson number for the wind component projected to the assumed azimuthal direction of wave propagation (solid line, observed Ri; dotted line, critical Ri).

4.3. WAVE FLUXES

Figure 7 shows an example of cospectra of momentum and heat fluxes for event A. Contributions from the wave motions to the fluxes clearly dominate over contributions from high frequency turbulence. Table III lists the minimum cospectral values ($\tilde{\tau}$ and $\tilde{H}$) and the corresponding phase angles for the two EC heights above the canopy. The ratios of $\tilde{\tau}$ and $\tilde{H}$ to the corresponding Reynolds statistics or the integrated cospectral energy (Table I) are in the range 3–18. To put this into perspective, the ratio of the cospectral peak to the total energy is about 0.3 for both momentum and sensible heat fluxes in a stable surface layer in the absence of waves (Figure 21 of Kaimal et al., 1972). The large difference is another manifestation of the importance of waves in canopy-air exchange processes.

In a phase domain, waves result in a positive flux (upward flux) if the phase angle between u and w or w and T is in the range -90° to 90°, and a negative flux

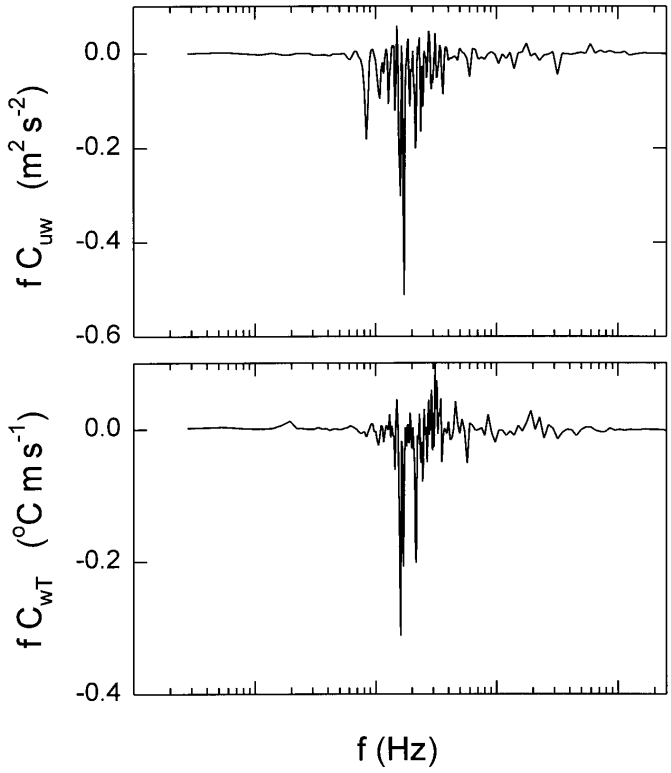

Figure 7. Example of cospectra of momentum flux (top) and sensible heat flux (bottom) at z = 27.7 m for event A.

(downward flux) otherwise. It is shown from linear analysis that the w–T phase angle is determined by the growth rate, wave number and difference in wind speed between the observation level and the critical level, as

$$\Phi_{wT} = \tan^{-1}[k(\overline{u} - c_r)/\sigma_i] \tag{7}$$

(de Baas and Driedonks, 1985). For waves generated in the upper boundary layer, the phase angle observed near the ground should be close to $\pm$ 90° as $\mid \overline{u} - c_r \mid$ is sufficiently large, and therefore waves should contribute little to the sensible heat flux. In the case of canopy waves, this angle is in general not equal to $\pm$ 90° (Table III) and large apparent fluxes of sensible heat and other constituents can result from wave motions (Table I; refer also to Lee et al., 1996). We suggest that the deviation from $\pm$ 90° is caused by the small difference between $\overline{u}$ and c_r and possibly by the canopy drag force imposed on the wavy wind as well.

Table III
Minimum cospectral values for momentum ($\tilde{\tau}$) and sensible heat ($\tilde{H}$) fluxes and phase angles (Φ_{uw}, Φ_{wT}) at the minimum frequencies at two EC observation levels over the forest

Event	z m	$\tilde{\tau}$ $m^2\ s^{-2}$	Φ_{uw} deg	$\tilde{H}$ $^\circ C\ m\ s^{-1}$	Φ_{wT} deg
A	39.1	−0.33	150	−0.37	−118
	27.7	−0.51	170	−0.31	−130
B	39.1	−0.04	157	−0.03	−121
	27.7	−0.25	156	−0.20	−149

5. Conclusions

A clear picture has emerged from the discussion above. The phase speed of canopy waves is rather low in comparison with waves in the upper boundary layer. Our best estimates for events A and B are 2.2 and 1.3 m s^{-1} respectively. The wave periods, 59 and 50 s for events A and B respectively, are also much smaller than the periods of waves in the upper boundary layer. These canopy waves are shallow (wave vertical displacement smaller than wavelength) and are ideal candidates for linear analysis.

There is strong evidence from the present analysis and from the literature supporting our postulate that canopy waves are generated by shear instability. We propose that wind shear near the inflection point of the mean wind profile, which occurs around the canopy top, is often large enough to reduce the gradient Richardson number to values less than the critical value of 0.25 and thus is able to trigger the instability. When external conditions are favorable, the instability will grow into waves. One may then argue that nighttime waves and coherent motions in neutral and unstable air belong to the same motion type in the sense that both are generated by shear instability. This explains why canopy wave periods and periods of coherent structures are similar in magnitude. A major difference is that coherent eddies are a result of the shear-generated waves that have undergone non-linear processes. At night, the ingredient of the non-linear processes, turbulence, is either absent or rather weak, so waves can retain their initial forms well described by the linear theory and therefore appear much cleaner than daytime coherent structures.

Acknowledgement

We appreciate the assistance with the experiment by J. Arnold, J. Deary, G. Edwards, Z. Nesic, and I. Simpson. Thanks also go to R. Staebler who provided invaluable help with the experiment and in managing the large volume of data. This work was supported in part by National Science Foundation Grant ATM-9629497.

References

Black, T. A., den Hartog, G., Neumann, H. H., Blanken, P. D., Yang, P. C., Russell, C., Nesic, Z., Lee, X., Chen, S. G., Staebler, R., and Novak, M. D.: 1996, 'Annual Cycles of Water Vapor and Carbon Dioxide Fluxes in and above a Boreal Aspen Forest', *Global Change Biology* **2**, 219–229.

Busack, B. and Brümmer, B.: 1988, 'A Case Study of Kelvin–Helmholtz Waves within an Offshore Stable Boundary Layer: Observations and Linear Model', *Boundary-Layer Meteorol.* **44**, 105–135.

Chimonas, G. and Hines, C. O.: 1986, 'Doppler Ducting of Atmospheric Gravity Waves', *J. Geophys. Res.* **91d**, 1219–1230.

de Baas, A. F. and Driedonks, G. M.: 1985, 'Internal Gravity Waves in a Stably Stratified Boundary Layer', *Boundary-Layer Meteorol.* **31**, 303–323.

Einaudi, F. and Finnigan, J. J.: 1993, 'Wave-Turbulence Dynamics in the Stably Stratified Boundary Layer', *J. Atmos. Sci.* **50**, 1841–1864.

Einaudi, F. and Finnigan, J. J.: 1981, 'The Interaction between an Internal Gravity Wave and the Planetary Boundary Layer. Part I: the Linear Analysis', *Quart. J. Roy. Meteorol. Soc.* **107**, 793–806.

Finnigan, J. J.: 1988, 'Kinetic Energy Transfer between Internal Gravity Waves and Turbulence', *J. Atmos. Sci.*, **45**, 486–505.

Finnigan, J. J., Euinaudi, F., and Fua, D.: 1984, 'The Interaction between an Internal Gravity Wave and Turbulence in the Stably-Stratified Nocturnal Boundary Layer', *J. Atmos. Sci.* **41**, 2409–2436.

Fitzjarrald, D. R. and Moore, K. E.: 1990, 'Mechanisms of Nocturnal Exchange between the Rain Forest and the Atmosphere', *J. Geophys. Res.* **95d**, 16,839–16,850.

Gossard, E. E. and Hooke, W. H.: 1975, *Waves in the Atmosphere*, Elsevier Scientific Publishing Company, Amsterdam, 456 pp.

Gossard, E. E. and Munk, W. H.: 1954, 'On Gravity Waves in The Atmosphere', *J. Meteorol.* **11**, 259–269.

Hooke, W. H., Hall, F. F., and Gossard, E. E.: 1973, 'Observed Generation of an Atmospheric Gravity Wave by Shear Instability in the Mean Flow of the Planetary Boundary Layer', *Boundary-Layer Meteorol.* **5**, 29–41.

Howard, L. N.: 1961, 'Note on a Paper of J. W. Miles', *J. Fluid Mech.* **10**, 509–512.

Kaimal, J. C., Wyngaard, J. C., Izumi, Y., and Coté, O. R.: 1972, 'Spectral Characteristics of Surface Layer Turbulence', *Quart. J. Roy. Meteorol. Soc.* **98**, 563–589.

King, J. C., Mobbs, S. D., Darby, M. S., and Rees, J. M.: 1987, 'Observations of an Internal Gravity Wave in the Lower Troposphere at Halley, Antarctica', *Boundary-Layer Meteorol.* **39**, 1–13.

Lee, X.: 1996, 'Turbulence Spectra and Eddy Diffusivity over Forests', *J. Appl. Meteorol.* **35**, 1307–1318.

Lee, X., Black, T. A., den Hartog, G., Neumann, H. H., Nesic, Z., and Olejnik, J.: 1996, 'Carbon Dioxide Exchange and Nocturnal Processes over a Mixed Deciduous Forest', *Agric. For. Meteorol.*, in press.

Maitani, T.: 1989, 'Wave-like Wind Fluctuations Observed in the Stable Surface Layer Over a Plant Canopy', *Boundary-Layer Meteorol.* **48**, 19–31.

Miles, J. W.: 1961, 'On the Stability of Heterogeneous Shear Flow', *J. Fluid Mech.* **10**, 496–508.

Nappo, C. J. and Chimonas, G. C.: 1992, 'Wave Exchange between the Ground Surface and a Boundary-Layer Critical Level', *J. Atmos. Sci.* **49**, 1075–1091.

Paw U, K. T., Brunet, Y., Collineau, S., Shaw, R. H., Maitani, T., Qiu, J., and Hipps, L.: 1992, 'On Coherent Structures in Turbulence above and within Agricultural Plant Canopies', *Agric. For. Meteorol.* **61**, 55–68.

Paw U, K. T., Shaw, R. H., Maitani, T., and Cionco, R. M.: 1989, 'Gravity Waves in an Almond Orchard', in *19th AMS Conf. Agric. For. Meteorol.* pp. 184–185 (preprint).

Raupach, M. R., Finnigan, J. J., and Brunet, Y.: 1989, 'Coherent Eddies in Vegetation Canopies', in *4th Australasian Conf. on Heat and Mass Transfer*, Christchurch, New Zealand, pp. 75–90.